Ecological Indicators 153 (2023) 110413

Contents lists available at ScienceDirect

Ecological Indicators

journal homepage: www.elsevier.com/locate/ecolind

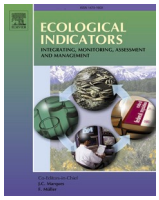

Original Articles

Increasing compound drought and hot event over the Tibetan Plateau and its effects on soil water

Di Wu [a,b,c], Zeyong Hu [a,b,*]

[a] Key Laboratory of Land Surface Process and Climate Change in Cold and Arid Regions, Northwest Institute of Eco-Environment and Resources, Chinese Academy of Sciences, Lanzhou 730000, China
[b] Nagqu Station of Plateau Climate and Environment, Northwest Institute of Eco-Environment and Resources, Chinese Academy of Sciences, Nagqu 852000, China
[c] University of Chinese Academy of Sciences, Beijing 100049, China

ARTICLE INFO

Keywords:
Compound drought and hot events
Joint probability
Conditional probability
Soil water scarcity

ABSTRACT

Climate extremes, such as droughts and hot events, are expected to become more frequent and intense as the Earth's climate continues to change. Indeed, they will likely pose increasingly serious threats to both humanity and the sustainability of natural ecosystems. Compound climate extremes may significantly impact regions sensitive to climate change, such as the Tibetan Plateau (TP), although there is currently a notable lack of research on compound extreme drought and hot events (CEDHs) that affect this region. We employed the copula model using the standardized precipitation index (SPI), standardized temperature index (STI), and standardized soil moisture index (SSMI) to explore patterns of changes in CEDHs and assess the risk of soil water scarcity under CEDHs. Our results showed that the probability of CEDHs increased significantly across the TP over time, mainly due to hot events becoming more common. The conditional probability of soil water scarcity (SSMI < -0.8) under moderate CEDHs (defined as SPI < − 0.8 and STI > 0.8) increased by 81.8% and 21.4% over time compared with those under individual hot and dry conditions, respectively. Our findings have important implications for mitigating the impacts of CEDHs under future global warming scenarios.

1. Introduction

Climate extremes (e.g. heat waves, cold waves, droughts, and floods) can cause significant damage to a region's agriculture, economy, water supply, ecosystem, and public health (Xiao et al., 2016; Lai et al., 2018; Kollanus et al., 2021), and such extreme events have become increasingly common over many land areas in recent decades due to warming of the climate (Perkins et al., 2012; Hao et al., 2018). This trend indicates that both civilization and the natural environment will face greater threats from future climate extremes; therefore, much research has been conducted on the spatiotemporal characteristics, driving factors, and effects of extreme events in order to understand how to mitigate these impacts (Fischer and Schär, 2010; Qin et al., 2015; Asong et al., 2018). Traditional researches into extreme events generally focuse on them as independent occurrences, whereby such studies tend to focus on extreme conditions for a single variable (e.g. temperature or precipitation); However, multiple extreme events have been documented to occur simultaneously in the same location in many areas around the world, which are referred to as compound climate extremes. For example, in 2018, there was a compound drought and hot event in Europe, and a compound flooding and hot event in Japan (Bastos et al., 2021; Wang et al., 2019b). In addition, compound extreme climates, which are defined as the combination of different statistically dependent variables, may have a greater impact than the effect of each climate event in isolation (Feng et al., 2021a, Feng et al., 2021b). Therefore, statistical methods limited to analyzing single climatic conditions likely underestimate the risks of those climate extremes that are compound extremes in nature (Chen et al., 2019a). As such, it is important to quantify the superimposed risks through multivariate physical and statistical frameworks.

The compound extreme drought and hot event (CEDH) is one of many compound extremes that could cause a series of extreme impacts on society and the environment. For instance, a CEDH affected large areas of Russia in the summer of 2010, which reduced annual crop production by 25% and caused an estimated 55,000 deaths, as well as causing>1 million hectares of crop failure and nearly 70,000 deaths across Europe. (Robine et al., 2008). The past decade witnessed a surge in the number of studies of CEDHs at both the global and the national

* Corresponding author at: CAS Center for Excellence in Tibetan Plateau Earth Sciences, Beijing 100101, China.
E-mail address: zyhu@lzb.ac.cn (Z. Hu).

https://doi.org/10.1016/j.ecolind.2023.110413
Received 28 October 2022; Received in revised form 13 April 2023; Accepted 22 May 2023
Available online 2 June 2023
1470-160X/© 2023 The Author(s). Published by Elsevier Ltd. This is an open access article under the CC BY-NC-ND license (http://creativecommons.org/licenses/by-nc-nd/4.0/).

scale (Zscheischler and Seneviratne, 2017; Kong et al., 2020). An increasing frequency and spatial extent of CEDHs were documented in many nations, such as China, the United States of America, and India (Beniston, 2009; Hao et al., 2020a; Feng et al., 2020; Ganguli, 2022), and the risks associated with CEDHs were projected to worsen under future climate warming scenarios of 1.5 and 2.0 °C (Liu et al., 2021).

The Tibetan Plateau (TP) covers an area of nearly 2.5 million km^2, has an average altitude above 4000 m, and is considered to be the largest and highest topographic plateau in the world. The TP and its surrounding regions contain several glaciers, large areas of frozen soil, inland lakes, and multiple ecosystems, which makes it highly sensitive to climate change (Wan et al., 2016, Li et al., 2020). Since its surface is close to the middle troposphere, land–atmosphere interactions on the TP are important processes that contribute to shaping the regional and global climate. The TP has experienced significant warming over the past five decades (Chen et al., 2015), which provoked several questions about how climate extremes would change across the region in the future. You et al. (2008) suggested that both daytime and nighttime hot events were becoming more common, with nighttime ones also thought to be more extreme than daytime ones. In addition, Yin et al. (2019) used CMIP5 experiments to study the role of human influence on temperature extremes across the TP; they showed that anthropogenic signals could be robustly detected in all extreme indices and that all show increasing trends. Li et al. (2019a) found that droughts were exacerbated in the humid southern part of the Yarlung Zangbo River Basin. Liu et al. (2022) investigated soil moisture droughts on the TP and their driving forces, and showed that Atlantic multi-decadal oscillations from cold to warm states could control precipitation on the TP, which consequently reduced the number of soil moisture-related drought events. Although much research has been performed on climate extremes on the Qinghai–Tibet Plateau, there are few researches on CEDHs, and it is critical to investigate CEDHs for its greater impacts. You et al (2021) reported that conducting additional studies of compound events was one of the most important directions for researching climate extremes on the TP. In addition, high temperature and low precipitation could significantly impose a negative impact on ecosystem on TP by inducing water stress on vegetation growth (Fu et al., 2013; Li et al., 2019b). Li et al. (2013) investigated the effect of soil moisture in southern TP and indicated that soil moisture content at depths of upper 60 cm was the key factor limiting the seed germination and seedling growth, and affecting vegetation coverage directly. Wang et al. (2016) also suggested the soil moisture and temperature were two main factors controlling growth of alpine steppe on TP. Furthermore, some previous literature showed that the content and distribution of soil moisture affected the restoration of degenerated ecosystems (Zhao, 2002; Qiu et al., 2007). Therefore, the potential risks to vegetation due to CEDHs-related soil water scarcity should also be assessed.

The current study aims to improve our understanding of CEDHs over the TP from a joint probability perspective. The primary objectives of this study are to: (1) investigate the spatial and temporal variations in probability of CEDHs on TP, whilst also identify the factors that contribute to these variations; and (2) assess the risk of soil water scarcity on the TP under CEDHs.

2. Study area and data

2.1. Study area

The study area considered here is located from 68° E to 106° E and 24° N to 42° N (Fig. 1a). The TP is colloquially known as the "Asian water tower", since it is a headwater region for many important rivers, such as the Yangtze River and the Yellow River. It can be further divided into 12 basins according to the locations of major rivers and lakes (Zhang et al., 2013): the Amu Dayra Basin (AB), the Brahmaputra Basin (BB), the Ganges Basin (GB), the Hexi Basin (HB), the Indus Basin (INDB), the Inner Basin (INNB), the Mekong Basin (MB), the Qaidam Basin (QB), the Salween Basin (SB), the Yangtze Basin (YAB), the Yellow Basin (YEB) and the the Tarim Basin (TB). The alpine grassland covering nearly two-thirds of the total plateau area is the dominant vegetation type on the TP, although some shrubs grow in the central–southern region and some forests grow along the southeastern corner (Li et al., 2020). Affected by terrain and South Asian monsoon, the climate of TP is characterized by thermal and moisture gradients from southeast to northwest (Sun et al., 2022). Generally, the TP has a climate characterized by low temperature, and limited water availability with respect to its high altitude.

2.2. Data sources

This study used the standardized precipitation index (SPI), standardized temperature index (STI), and the standardized soil moisture index (SSMI) to monitor meteorological droughts, hot events, and soil water scarcity, respectively. They were calculated by precipitation, temperature and soil moisture respectively.

In order to make the research results more credible, three sets of gridded monthly precipitation data were used in this study. The first one from 1891 to 2019 with a spatial resolution of 0.25° was derived from the Global Precipitation Climatology Centre (GPCC V2020) (https://psl.noaa.gov/data/). The second one from 1901 to 2020 with a spatial resolution of 0.5° was obtained from the Climatic Research Unit (CRU

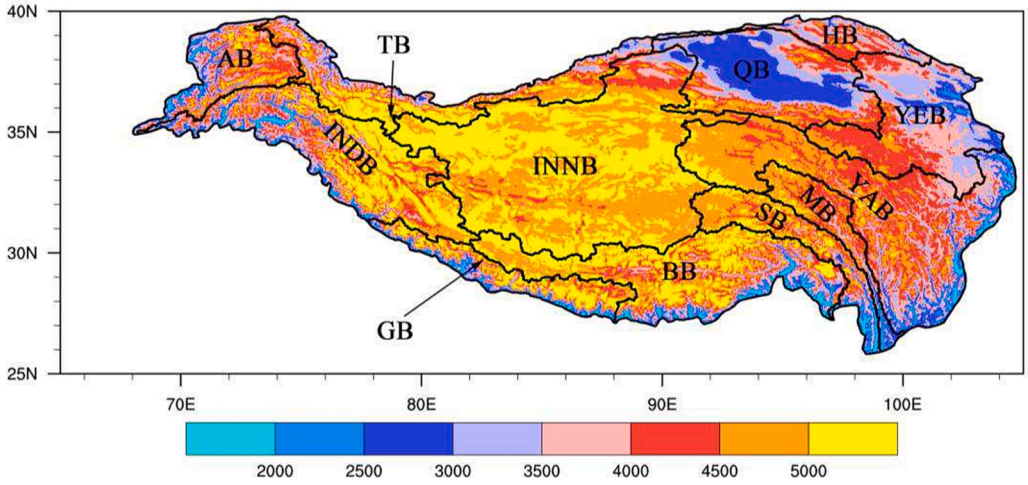

Fig. 1. Map of the TP showing the location of basins.

TS4.05)(https://www.cru.uea.ac.uk/cru/data/). The third one from 1948 to 2014 with a spatial resolution of 0.25° was provided by Princeton Global Meteorological Forcing Data (PMFD) (Sheffield et al., 2006) and was obtained at https://disc.gsfc.nasa.gov/dataset/. Besides, two sets of gridded monthly temperatures data employed in this study were also derived from the CRU TS4.05 climate datasets and PMFD, respectively.

Three sets of root zone soil moisture data were respectively simulated by NOAH land surface model, Variable Infiltration Capacity (VIC) land surface model and Catchment Land Surface Model (CLSM). During the simulation, PMFD still served as atmospheric forcing to drive land surface model. The monthly root zone soil moisture from 1948 to 2014 with a spatial resolution of 0.25° were obtained from the Global Land Data Assimilation System (GLDAS-2) (https://disc.gsfc.nasa.gov/datasets).

The dataset for river basins across the TP was adapted from previous studies (Zhang et al., 2013; Zhang, 2019) and was available at https://data.tpdc.ac.cn.

All of these datasets were widely used for the study of climate change and hydrological processes on the TP, primarily due to their broad spatial coverage and reliability (Yang et al., 2018; Bai et al., 2019; Hua and Wang, 2018; You et al., 2019; Wang et al., 2021c; Wei et al., 2022). Due to the different coverage periods and resolutions of each data, some works to solve this question were as follows: First of all, the study period 1951–2014 was selected for this study, since climate datasets(GPCC, CRU and PMFD) merged site observation, however substantive meteorological observations over the TP only initiated during the 1950 s (Shi et al., 2019). Secondly, all data was interpolated to 0.5° resolution by bilinear interpolation. Additionally, we only focused on climate in summer (June–July–August) for two reason: (1) summer is not only the hottest season but vegetation growing season; (2) the precipitation on the TP is mainly concentrated in summer (Lin et al., 2021) and vegetation will be threatened by lack of summer precipitation. Thus, summer precipitation, average summer temperature and average summer soil moisture were used to calculated SPI, STI and SSMI. As shown in Fig. S1, three sets of precipitation data presented consistent summer precipitation changes over the TP (correlation coefficient from 0.87 to 0.94) and two sets of temperature data also exhibited consistent variations (correlation coefficient was 0.97). Finally, three pairs of climate datasets(.i.e precipitation from GPCC& temperature from CRU; precipitation from CRU& temperature from CRU; precipitation from PMFD& temperature from PMFD) were used to investigate variations in CEDHs and three pairs of climate-soil datasets (.i.e temperature and precipitation from PMFD & soil moisture from three land surface models) were employed to assess the risk of soil water scarcity under CEDHs. The results were calculated with each pair of datasets, and the averaged results would be given in the text.

3. Methodology

3.1. Drought, hot event and soil mositure indices

The SPI was calculated in two steps: 1) we estimated the actual distribution according to the empirical probability distribution function (Gringorten, 1963) (eq. (1), which avoided bias introduced by assuming a distribution function and also simplified the calculation (Hao et al., 2018); and 2) transformed the empirical distribution function into a normal distribution based on the normal quantile transformation (NQT) (Bogner et al., 2012), with the value of SPI calculated from precipitation data at each time step (eq. (2). The time scale of SPI was essentially 1 month in this study.

$$P(x_i) = \frac{n_i\text{--}0.44}{n + 0.12} \tag{1}$$

$$SPI_i = \Phi^{-1}hFhx_ihh \tag{2}$$

here, X represents precipitation, n_i is the number of occurrences when $X < x_i$, Φ^{-1} is the inverse function of the normal distribution, and F is the empirical distribution of X.

STI was calculated in a similar way to SPI, but using temperature data instead of precipitation data. The lower value of SPI, the more severe the drought. Thus, moderate, severe, and extreme meteorological droughts occur when SPI was less than the thresholds − 0.8, −1.3, and − 1.6, respectively, which approximated the 21.2, 9.7, and 5.5 percentiles in standard normal distribution (Feng et al., 2019). On the contrary, the value of STI, the more severe the hot event. Moderate, severe, and extreme hot events occurred when STI was greater than the thresholds 0.8, 1.3, and 1.6, respectively. CEDHs were defined as concurrent droughts and hot events, and were also divided into moderate (SPI $<$ − 0.8 and STI $>$ 0.8), severe (SPI $<$ − 1.3 and STI $>$ 1.3), and extreme (SPI $<$ − 1.6 and STI $>$ 1.6) levels. As climate change signals on long-term trends could influence temperature and precipitation, SPI and STI were also calculated using linearly detrended precipitation and temperature data in order to know how CEDHs changed without long-term trends (Zscheischler and Seneviratne, 2017; Chen et al., 2019a).

SSMI was also calculated in a similar way to SPI, but only detrended average summer soil moisture were employed. Similar to threshold of SPI, the value −0.8 was also selected as the threshold of SSMI to represent soil water scarcity. All thresholds and corresponding probabilities were shown in Table 1.

3.2. Bivariable probability analysis with copula model

To estimate the probability of CEDHs, copula model was employed to construct the joint distribution function of SPI (denoted as X) and STI (denoted as Y) to derive the compound event, which is written as:

$$P\{ X < x, Y > y\} = F_Y(y)\text{--}C(F_X(x),\ F_Y(y)) \tag{3}$$

Here, x and y are thresholds of SPI and STI, respectively, as mentioned above, and $F_X(x)$ and $F_Y(y)$ indicate the marginal non-exceedance probability distribution of SPI and STI, respectively. The marginal distribution of SPI and STI could be regarded as a normal distribution for the reason that calculating them using the normal quantile transformation (NQT). The copula (C) is a joint cumulative distribution function (CDF) that fits the joint dependence structure of two variables (i.e. SPI and STI) (Nelsen, 2007). Copula have a variety of families with different forms and parameters, which makes it straightforward to accurately characterize the relationships between two variables. Following the results of previous research (e.g. Zscheischler and Seneviratne, 2017; Manning et al., 2019), the normal Copula, t Copula, clayton Copula, gumbel Copula, and Frank Copula families were chosen in this study. We chose the best model according to the minimum value of the Aikaikes information criterion (AIC) at each grid point. The goodness of fit of copulas was tested using the "white" process (White, 1982; Huang and Prokhorov, 2014) via the "VineCopula" R packages. The selected copula family was rejected if the p-value was less than 0.05, which defined the acceptable range of tests that may fail by random chance (Manning et al., 2019).

Table 1
Definition of Climate Extremes and soil water scarcity.

Categories	Thresholds	Cumulative probability
Moderately dry	SPI $<$ -0.8	0.212
Severely dry	SPI $<$ -1.3	0.097
Extremely dry	SPI $<$ -1.6	0.055
Moderately hot	STI $>$ 0.8	0.212
Severely hot	STI $>$ 1.3	0.097
Extremely hot	STI $>$ 1.6	0.055
soil water scarcity	SSMI $<$ -0.8	0.212

3.3. Contributions to probability variation

The method proposed by Bevacqua et al. (2020) was used to quantitatively reveal the relative contribution of SPI and STI, alongside their dependence on variations of CEDHs between the two periods 1951–1982 and 1983–2014. This method works by designing three experiments to quantify how the joint probability of CEDHs changes between two periods when only one factor (i.e. SPI, STI, and their dependence) can vary. The difference of joint probability between each experiment (i) and control group can be written as follows (eq. (4):

$$\Delta PRO_{expi} = PRO_{expi} - PRO_1 \tag{4}$$

here, PRO_1 is the joint probability for the early period (i.e. 1951–1982) and PRO_{expi} is the joint probability computed by the three experiments described below.

Experiment 1: given the variable SPI1 (i.e. the value of SPI in the early period), we estimated the associated empirical CDF(U_{SPI1}). Given the variable SPI2 (i.e. the value of SPI in the late period), we defined the empirical CDF(F_{SPI2}), SPIexp1 = $F^{-1}_{SPI2}(U_{SPI1}(SPI1))$ was obtained through transformation by equal probability, and (SPIexp1, STI1), whose dependence is the same as that of (SPI1, STI1), was used to compute the joint probability via eq. (3). Notably, (SPIexp1, STI1) used the marginal distribution of SPI2 and the marginal distribution of STI in the early period to reflect the influence of changes in SPI on the return period variation.

Experiment 2: the contribution of STI to variations in CEDHs was surveyed using the procedure described in Experiment 1, but by considering temperature data instead of precipitation data.

Experiment 3: the contribution from SPI–STI dependence was quantified by using the bivariate variables (SPI1, STI1) and (SPI2, STI2) to compute the empirical CDF (i.e. SPIexp3 = $U^{-1}_{SPI1}(F_{SPI2}(SPI2))$ and STIexp3 = $U^{-1}_{STI1}(F_{STI2}(STI2))$). The variables (SPIexp3, STIexp3) have the same dependence as (SPI2, STI2), while have the same marginal distribution as (SPI1, STI1).

Thus the contribution of each variable was calculated as follows:

$$contribution_i = \frac{\Delta PRO_{expi}}{|\Delta PRO_{exp1}| + |\Delta PRO_{exp2}| + |\Delta PRO_{exp3}| + |offset|} \tag{5}$$

here, PRO_1 and PRO_2 are the joint probability of CEDHs in the early and late periods, respectively; and ΔPRO_{exp1}, ΔPRO_{exp2}, and ΔPRO_{exp3} are the variations of joint probability arising from the change of SPI, STI, and their dependence, respectively. It is known that the sum of ΔPRO_{exp1}, ΔPRO_{exp2}, and ΔPRO_{exp3} may not always be equal to PRO_2 - PRO_1; Thus, an offset was introduced as follows:

$$offset = PRO_2 - PRO_1 - \Delta PRO_{exp1} - \Delta PRO_{exp2} - \Delta PRO_{exp3} \tag{6}$$

3.4. Multivariate probability analysis with the vine copula model

Vine copulas are effective tools for modeling flexible dependence in large numbers of dimensions (.i.e three dimensions or higher) where the other copula families mentioned above may no longer work. The construction of a vine copula involves a process called “pair copula constructions” (PCCs), where n(n − 1)/2 bivariate copula densities were selected to constitute an n-dimensional multivariate density (eq. (4). Additionally, there are n − 1 trees in a vine copula that indicate how these variables link with each other (Aas et al., 2009). There are two general types of vine copulas: canonical vines (C-vines) and drawable vines (D-vines). In this study, we used C-vines to construct the joint distribution of detrended SPI, STI, and SSMI, and then assessed the risk of water soil water scarcity caused by CEDHs. The conditional probability of soil water loss below the prescribed threshold (i.e. −0.8) under a CEDH can be expressed as:

$$\begin{aligned} &P(SSMI < threshold_{SSMI} | SPI < threshold_{SPI} \& STI > threshold_{STI}) \\ &= P(SSMI < threshold_{SSMI} | SPI < threshold_{SPI} \& -STI < -threshold_{STI}) \\ &= \frac{F(threshold_{SSMI}, threshold_{SPI}, -threshold_{STI})}{C(threshold_{SPI}, -threshold_{STI})} \end{aligned} \tag{7}$$

here, −STI is the inverse value of STI, C represents the bivariate copula distribution function of SPI and STI, and F is the joint distribution of detrended SPI, STI, and SSMI. Furthermore, the marginal distribution of SPI, STI and SSMI is normal distribution. Previous researches provided more detailed information about these calculations (Aas et al., 2009; Li et al., 2021; Zhu et al., 2021a), and we performed these using the R package “Vines”.

Fig. 2 presented the framework of copula-based probabilistic analysis. Obviously, the calculation of probability of CEDHs and assessment of risk of soil water scarcity under droughts or hot events were bivariate cases, while the vine copula was employed to estimate the risk of soil water scarcity caused by CEDHs, and it was a trivariate case.

3.5. Kendall rank correlation coefficient

The Kendall rank correlation coefficient was used to evaluate the degree of rank similarity between two sets of observations, such as SPI and STI in this study. This coefficient depends upon the concept of concordance. For example, if (Xj − Xi) (Yj − Yi) > 0, then (Xi, Yi) and (Xj, Yj) are concordant, and they have the same tendency; conversely, if (Xj − Xi) (Yj − Yi) less than 0, then (Xi, Yi) and (Xj, Yj) are discordant, it is appropriate to measure the dependence between SPI and STI.

4. Results

4.1. Dependence between precipitation and temperature, and the probability of CEDHs

The spatial distribution of correlation coefficient between summer precipitation and temperature is shown in Fig. 3a. Approximately 26.6% of regions on the TP showed positive dependence between precipitation and temperature, and the remaining 73.4% showed negative dependence. The positive dependence were mainly located in the, QB, YEB, and could also be found in parts of YAB, MB, SB and INNB. All other regions showed negative dependence, although the significant correlation was only in the southern part of the TP. A negative dependence signified that low precipitation rates were often accompanied by high temperatures, as observed in many parts of world (Kong et al., 2020; Wu and Jiang, 2022). The underlying physical mechanism for this relationship were shown by previous studies to be land–atmosphere interactions (if precipitation exhibits a strong negative anomaly for several months, soil moisture will decrease continuously due to evaporation and the lack of water replenishment. Then, reduced soil moisture will limit evaporation and convert most incoming solar radiation to sensible heat, which warms the atmosphere. Additionally, low precipitation often corresponds to low cloud cover, which increases incident radiation and supplies energy for heating the atmosphere. The high temperatures can then prolong soil drought conditions (Zscheischler and Seneviratne, 2017; Wang et al., 2021c; Zhang et al., 2022)). Positive dependence were also reported in some studies, although their causative physical mechanism was poorly understood. A possible mechanism proposed by Fang et al. (2015) was that increased temperature might stimulate the emissions of biogenic volatile organic compounds (BVOC) from terrestrial vegetation on the TP, which increased the number of cloud condensation nuclei in the atmosphere (SOA), leading to increased precipitation and further vegetation growth. This was an important mechanism, as there are fewer aerosols on the TP compared to low-altitude regions.. Except for land–atmosphere interactions, long-term climate trends for precipitation and temperature could also cause

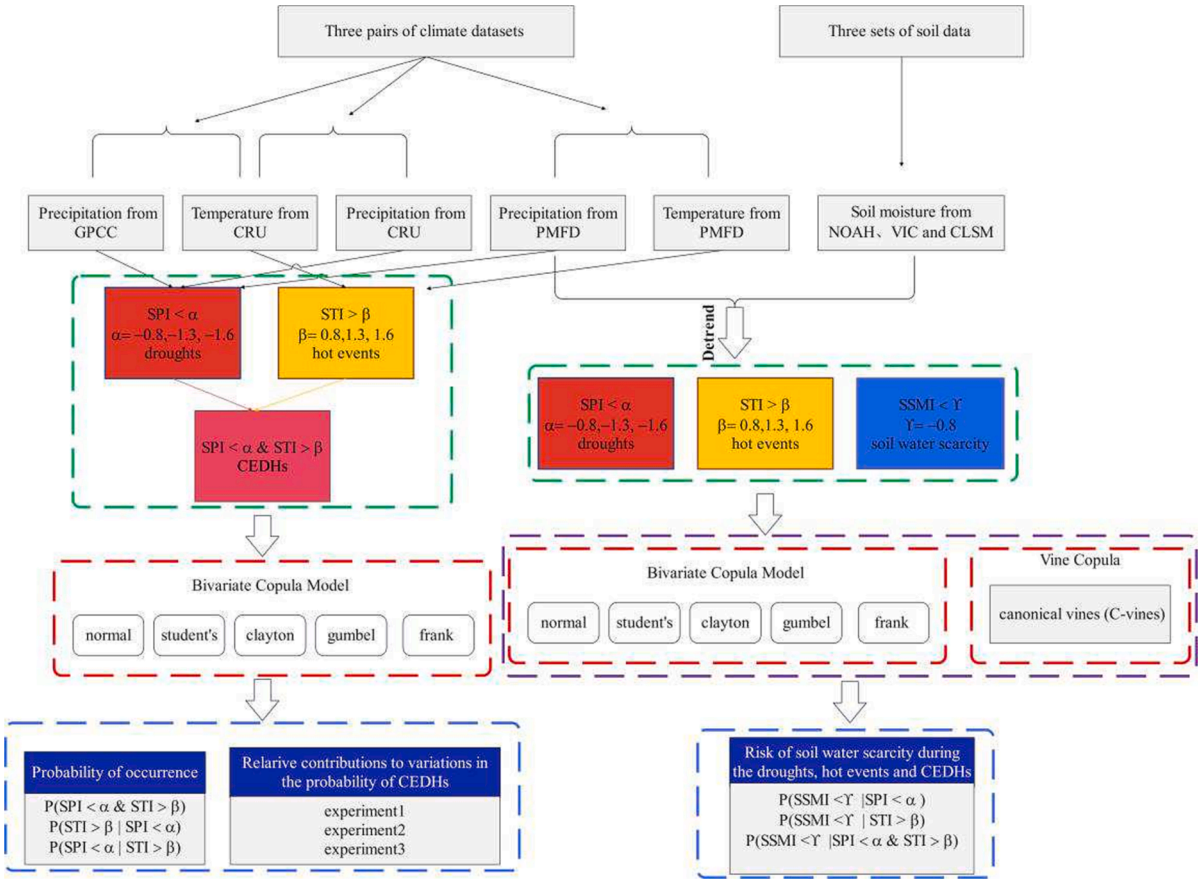

Fig. 2. Framework of copula-based analysis for estimating the probability of CEDHs and assessing the risk of soil scaricity.

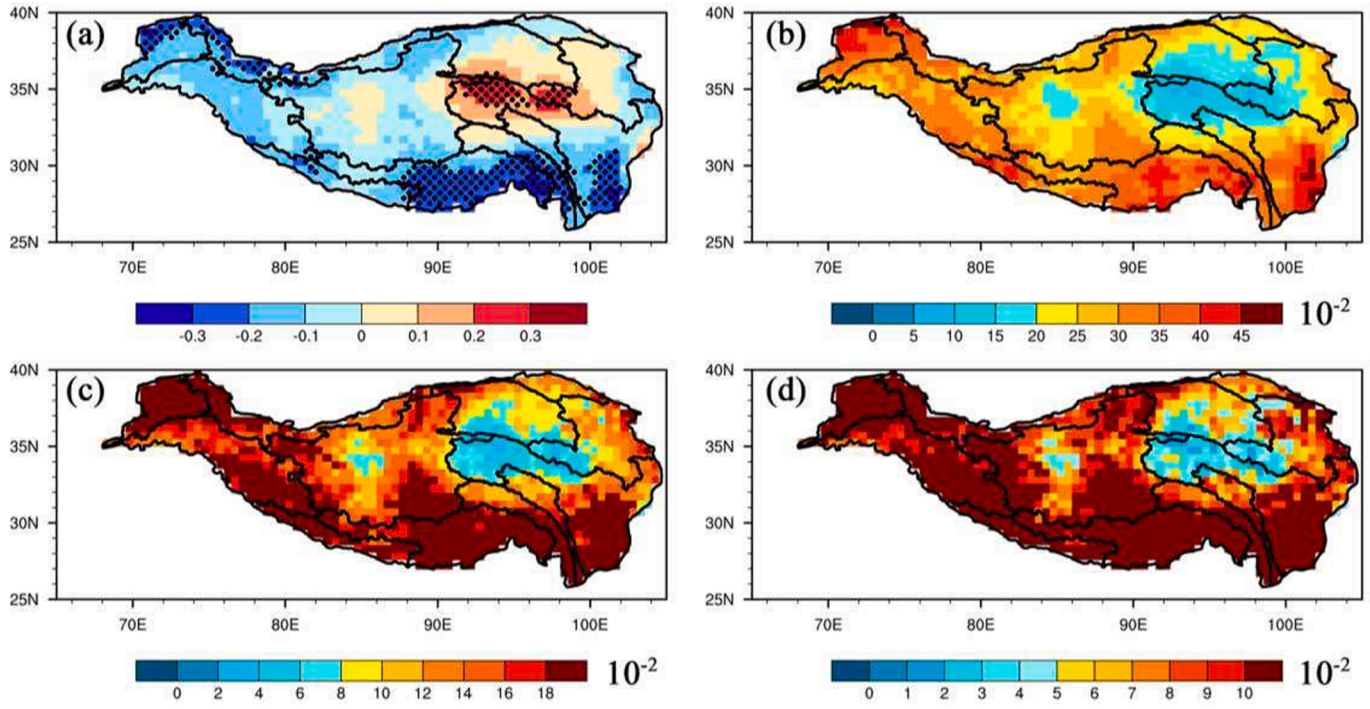

Fig. 3. The Kendall correlation between (a) precipitation and temperature, and the conditional probability P (STI > thresholdSTI | SPI < thresholdSPI) for (b) moderate, (c) severe, and (d) extreme severity levels. The average over all datasets was shown. Stippling highlights locations where the correlation was significant.

positive dependence. As shown in Fig. S2, more regions exhibited a significant negative dependence after applying a detrending algorithm to precipitation and temperature data. The spatial distribution of the conditional probability P (STI > thresholdSTI | SPI < thresholdSPI) for moderate, severe, and extreme events showed similar patterns to dependence (Fig. 3b–d). For example, the probability for moderate severity was less than 0.2 in regions with a positive dependence, but was>0.2 in regions with a negative dependence. It should be noted that the probability for a moderate level of severity should be 0.212, when temperature and precipitation are completely independent variables. This suggested that the dependence have clear impacts on CEDH, which had also been concluded by some previous studies (Zscheischler and Seneviratne, 2017; Hao et al., 2019; Wu and Jiang, 2022). Moreover, the results obtained from different datasets were similar to the above and further demonstratesd the reliability of the above results (Fig. S2-S3).

4.2. *Variations in the probability of droughts and hot events, and the dependence between precipitation and temperature*

The 64-year period considered here (1951–2014) was divided into two shorter periods with equal length for easy comparison (i.e. 1951–1982 and 1983–2014), as this approach of dividing period had been adopted by the exiting study (Hao et al. 2020a; Hao et al., 2020b, Wang et al., 2021b). The probability of droughts with different severity were calculated in each of these periods, as shown in Fig. 4 and Fig. S4-7. Given that droughts with different severity exhibited consistent changes, only variations in moderate droughts are discussed. Moderate droughts on the TP showed some variations in spatial heterogeneity, and the average probability of droughts showed a rise in the BB, GB, MB and SB, but a decrease in the other eight basins. The GB showed the largest probability increase (from 0.14 to 0.26) and the AB presented the largest probability reduction (from 0.29 to 0.13). In a word, both increase and decrease in probability of droughts on TP were significant (variations in all basins passed the Wilcoxon rank-sum test at 95% confidence level). The variations in probability for hot events showed a clear spatial consistency and the probability in all basins experienced a significant increase, which was consistent with the results reported by Yin et al. (2019). The INNB showed the largest increment from 0.07 to 0.36 (Fig. 5). The warming trends across the whole TP coupled with increasing precipitation in most basins could mainly explain variations in the probability of droughts and hot events. (Fig. S8). The variations in dependence between precipitation and temperature were shown in Fig. 6. During the former period, the basins except the YEB all exhibited a negative dependence, and a relatively strong negative dependency was observed in the AB, BB, and TB, with average correlation coefficients of −0.31, −0.25, and −0.29, respectively. During the latter period, the correlation coefficient increased significantly (negative dependence weakened) in 7 basins. For instance, negative dependence in the AB, BB, INNB, SB and TB weakened, while negative dependence in the MB, and QB became weak positive dependence; However, negative dependence

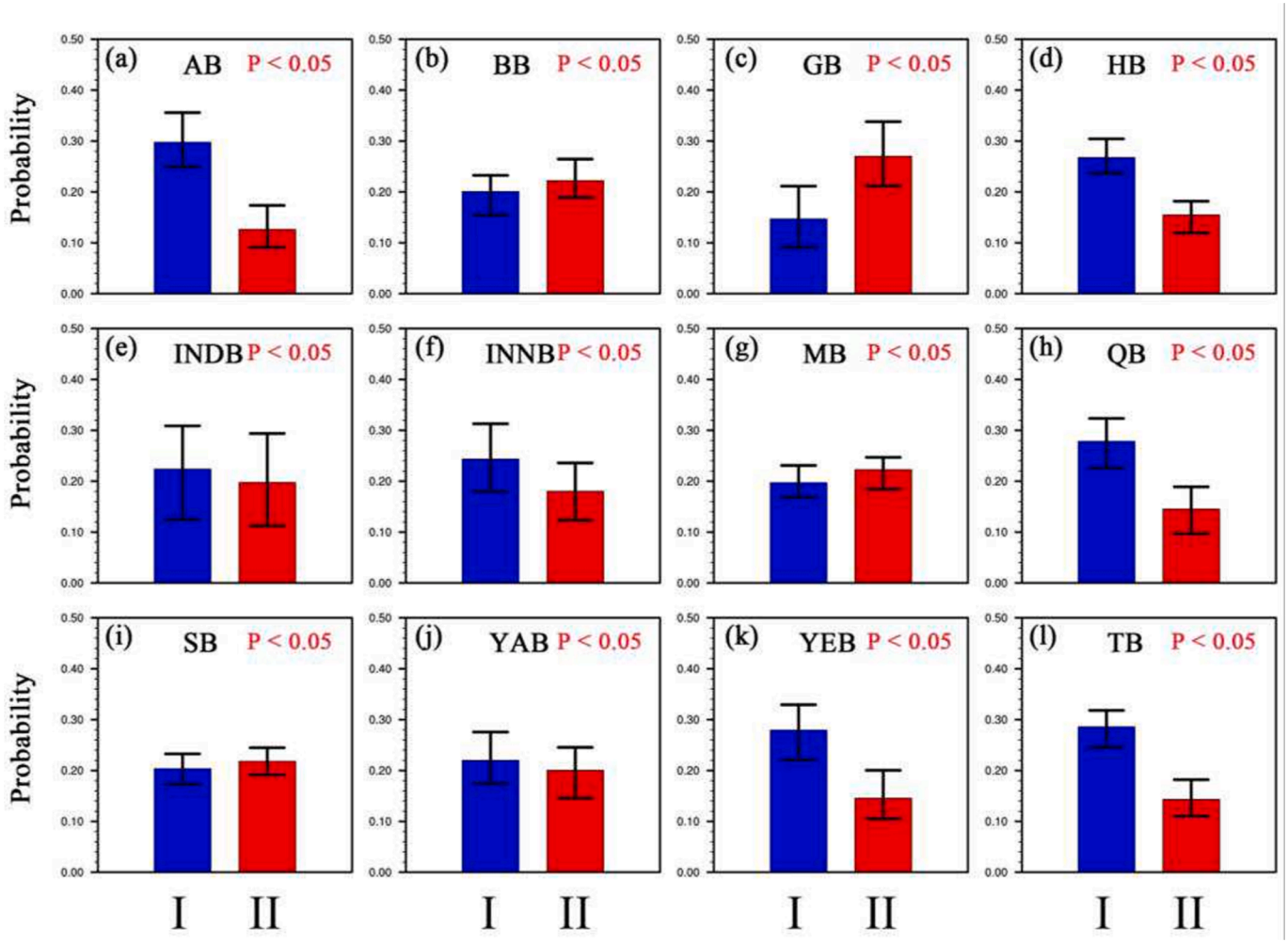

Fig. 4. The probability of moderate droughts in the periods 1951–1982 and 1983–2014. The average over all datasets was shown.Abbreviations were as follows: I, the period 1951–1982; II, the former period 1983–2014. P indicated the p-value from Wilcoxon rank-sum test and the p-values less than 0.05 indicated the variations in probability between two periods was significant. Error bars denoted the 5th and 95th percentiles.

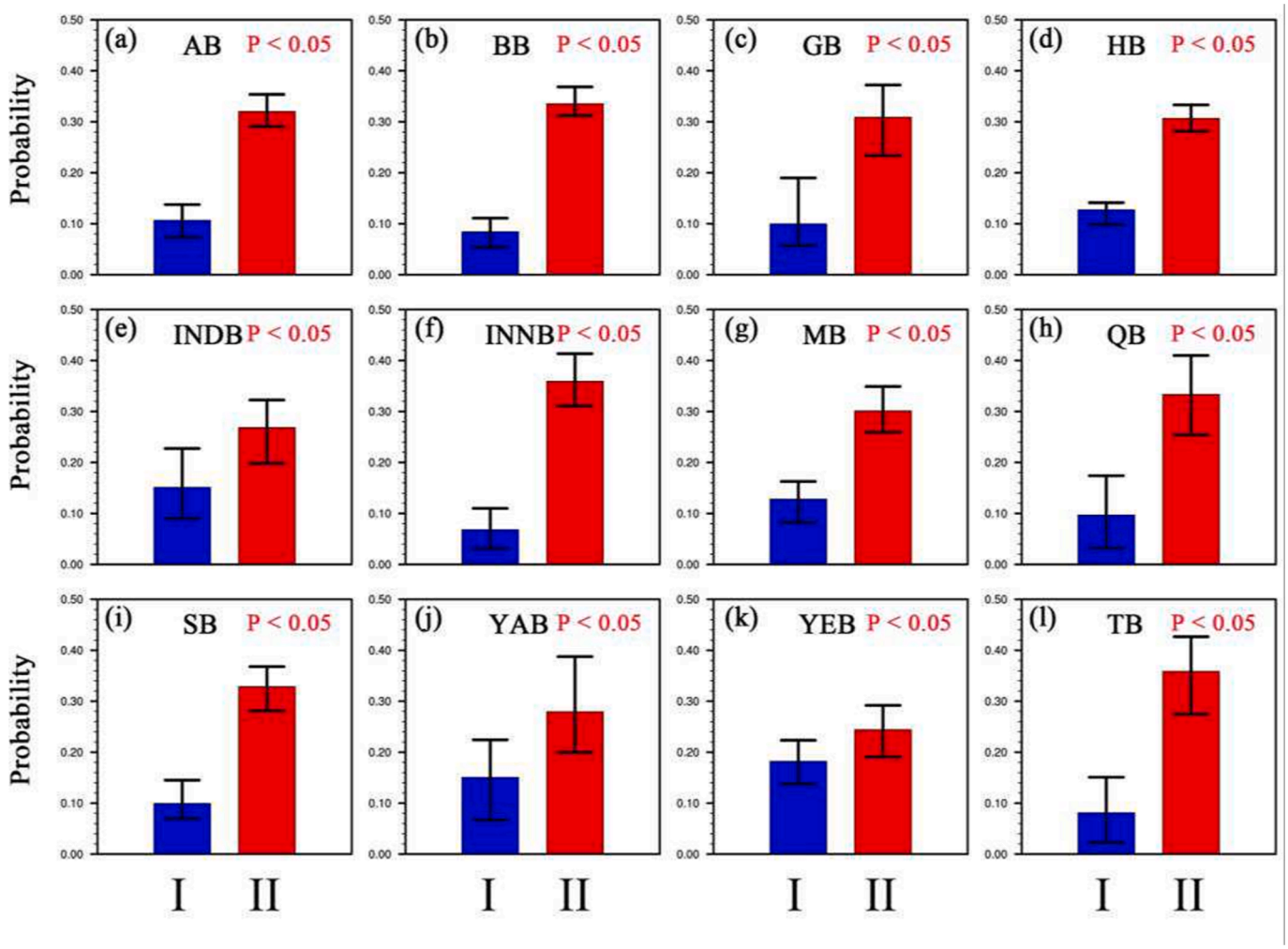

Fig. 5. The probability of moderate hot events in the periods 1951–1982 and 1983–2014. The average over all datasets was shown.Abbreviations were as follows: I, the period 1951–1982; II, the former period 1983–2014. P indicated the p-value from Wilcoxon rank-sum test and the p-values less than 0.05 indicated the variations in probability between two periods was significant. Error bars denoted the 5th and 95th percentiles.

were found to strengthen in the INDB and YEB.

5. Variations in the probability of CEDHs and their relative contributions

The probabilities of moderate CEDHs in both studied periods were shown in Fig. 7. In the former period, only 4 out of 12 basins (.i.e AB, BB, INDB and TB) exhibited larger probabilities than the joint probability of independent droughts and hot events (.i.e 0.044). The largest probability (0.07) were found in AB. This could be partly due to negative the dependence in these basins, although might also be influenced by the different distribution of SPI and STI between two periods, which caused the probability to deviate away from the threshold of 0.212. Except for AB, the probability of CEDHs significantly increased in all basins in the latter period. The largest increase occurred in the GB, with a value of 0.02 in the former period increasing by 0.1 to 0.12 in the latter period. Table 2 suggested that STI made the most important contributions (from 34.9% to 74.4.0%) to increasing the probability of CEDHs in all basins except for YEB. Indeed, 8 out of 12 basins exhibited contributions made from STI exceeded 50%, which was related to the overall rise in probability of hot events. The SPI made both positive and negative contributions (from −25.1% to 17.4%), although most basins showed a negative contribution, which was consistent with the drop in probability of droughts occurring in these basins. Dependence made negative contributions to the increasing of CEDHs in 8 basins, while the phenomenon that dependence turned from positive to negative in YEB was regarded as the main reason for the increase of probability of CEDHs in this region. This result highlighted the role of dependence in formation of CEDHs under the context of climate change, even if temperature appeared to be more influential in most basins. The contributions for severe and extreme CEDHs presented similar spatial patterns to those for moderate CEDHs (Fig. S9). In general, temperature had a dominant positive influence on the increase in CEDHs during periods of warming, while precipitation and dependence variations exerted both positive and negative influence on CEDHs to a certain extent, which was consistent with results reported by other studies (Hao et al., 2013; Mazdiyasni and AghaKouchak, 2015; Zhang et al., 2022). This phenomenon further led to a great asymmetric increase in the conditional probability of hot under dry conditions (P (STI > thresholdSTI | SPI < thresholdSPI)) and that of dry under hot conditions (P (SPI < thresholdSPI | STI > thresholdSTI)). As shown in Fig. 8, the number of grid points with increasing conditional probability of hot under dry conditions accounted for 98.6%, 95.6% and 93.4% for different severity level, while the number of grid points with increasing conditional probability of dry under hot conditions only accounted for 18.9%, 24.8% and 28.3%.

Detrended SPI and STI values were calculated by using detrended precipitation and temperature data in order to measure the contributions of variations in precipitation, temperature, and dependence without the influence of long-term trends. Variations in the probability of moderate CEDHs under a detrended scenario were shown in Fig. 9,

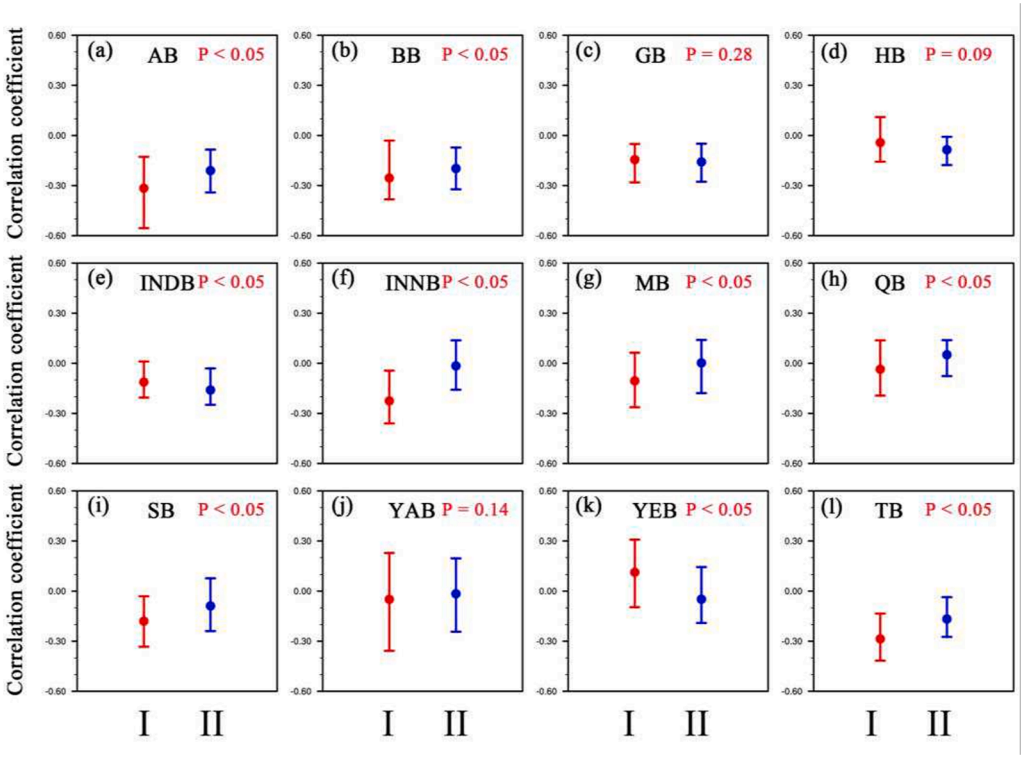

Fig. 6. The Kendall correlation between SPI and STI in two periods. The average over all datasets was shown. Abbreviations were as follows: I, the period 1951–1982; II, the former period 1983–2014. P indicated the p-value from Wilcoxon rank-sum test and the p-values less than 0.05 indicated the variations in probability between two periods was significant. Error bars denoted the 5th and 95th percentiles.

which was notably different from the previous result. Specifically, 11 out of 12 basins exhibited larger probabilities than the joint probability of independent droughts and hot events (.i.e 0.044). Besides, 8 out of 12 basins (.i.e GB, HB, INDB, INNB,QB, YAB, YEB and TB) presented a significant increased probability, while 2 basins (the AB and MB) showed a significant decreasing probability, with the greatest reduction (from 0.12 to 0.08) occurring in AB. The relative contributions are shown in Table 3, the factor contributing most to the variations in probability varied among basins; Compared with the other two factors (. i.e SPI and dependence), STI made largest (negative) contributions in AB, MB and YAB, but the probability of CEDH in YAB still showed a rise, which was because of the positive contributions made by both SPI and dependence. The SPI made largest (positive) contributions in GB, INNB, QB, SB and TB, however the probability in SB exhibited a non-significant decrease for nearly equal negative contributions made from two other factors (STI and dependence). As for dependence, it contributed most in HB, INDB and YEB, which then resulted in the rise of the probability there. In a word, all three factors could significantly affect the probability of CEDH, but none of them were dominant. It is well known that climate change is often associated with large-scale circulation anomalies and dependence generally depends on land–atmosphere feedback. Thus above results highlighted the equal important role that large-scale circulation and local land–atmosphere feedback played in variations of CEDHs when climate systems adapted to mean climate change. Additionally, the offset exhibited some large negative values in some regions such as HB, INDB, INNB and QB, which indicated summing the variations in probability induced by every factor might overestimate the actual changes in probability for these basins.

5.1. *Changes in type of climate extremes with long return periods*

In this section, return period was defined as the reciprocal of the joint probability. The return periods were calculated each year from 1951 to 2014, and events in each basin with a return period>20 years were identified. A return period of 20 years was chosen for the extreme events associated with this level are often highly destructive. The average values of SPI and STI for those events whose return period were>20 years were shown in Table 4. In the early period, the value of SPI in all basins was greater than the STI. The minimum and maximum values for SPI occurred in the AB (-1.70) and the YEB (-0.96), respectively, which indicated that selected events in all basins could readily achieved a minimum severity level representative of moderate drought (-0.8). Nonetheless, 10 out of 12 basins show the values of STI. lower than 0.8 (the threshold of moderate hot events). The low value of SPI combined with low value of STI mean that droughts were the main reason for high severity of events (return period > 20 years), while high temperatures played a smaller role in determining severity of events in former period. In the latter period, the values of SPI in all basins were smaller than values of STI. The SPI showed a total range of −1.16–-0.50, with 7 out of 12 basins reaching the minimum level required for moderate droughts, while the values of STI in all basins reached the minimum level required for moderate temperature extremes (0.8). The maximum value of STI (1.65) occurred in the AB and the minimum value of STI (1.04) occurred in the MB. This suggested that high temperatures determined severity of events in the HB, INNB, QB, YEB, and TB,and that high temperatures and low precipitations can both determine severity of events in the other seven basins in latter period. The results for those events whose return period were>30 years also presented similar patterns (Table S1). As a result, the climate extremes with long return periods on the TP generally experienced a transformation from droughts to hot events or CEDHs.

5.2. *The risk of soil water scarcity under droughts, hot events, and CEDHs.*

The risk of soil water scarcity caused by droughts, hot events, and CEDHs was assessed by calculating the conditional probabilities P (SSMI < thresholdSSMI | SPI < thresholdSPI), P (SSMI < thresholdSSMI | STI > thresholdSTI), and P (SSMI < thresholdSSMI | SPI < thresholdSPI, and

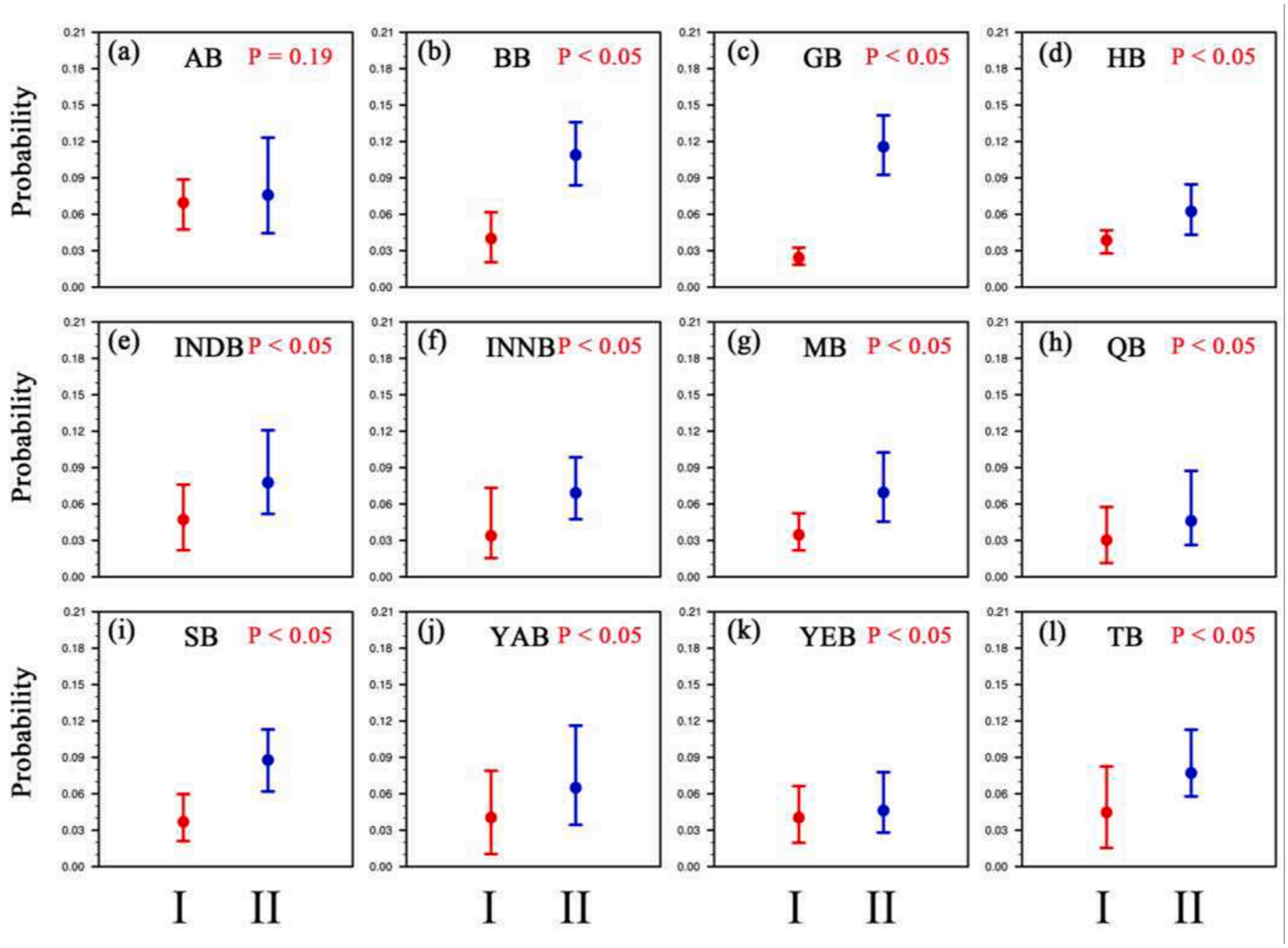

Fig. 7. The joint probability of CEDHs during two periods.The average over all datasets was shown. Abbreviations were as follows: I, the period 1951–1982; II, the former period 1983–2014. P indicated the p-value from Wilcoxon rank-sum test and the p-values less than 0.05 indicated the variations in probability between two periods was significant. Solid dots indicate the average probability.

Table 2
Relative contributions (%) to variations in CEDHs. The red numbers indicate the most contributions among the SPI, STI and dependence.

Basins	STI	SPI	Dependence	Offset
AB	50.7%	−15.1%	−4.1%	−27.9%
BB	72.1%	2.4%	−6.6%	2.6%
GB	41.4%	17.4%	3.7%	27.7%
HB	50.5%	−14.3%	7.8%	−21.5%
INDB	34.9%	−9.2%	13.3%	0.4%
INNB	60.9%	−3.0%	−8.3%	−24.0%
MB	67.7%	8.3%	−12.7%	−4.3%
QB	54.6%	−13.6%	−3.8%	−26.1%
SB	74.4%	4.8%	−8.0%	−5.5%
YAB	50.5%	−4.3%	−6.1%	−8.8%
YEB	17.9%	−25.1%	33.9%	−15.1%
TB	57.4%	−9.6%	−2.7%	−28.7%

STI > thresholdSTI), respectively. The risk facotrs (.i.e conditional probabilities) for moderate climate extremes in all basins were shown in Fig. 10. The conditional probability P (SSMI < thresholdSSMI | SPI < thresholdSPI) ranged from 0.38 to 0.64 and P (SSMI < thresholdSSMI | STI > thresholdSTI) ranged from 0.29 to 0.42. All of these values exceed a value of 0.212, which was the threshold that defines no relationship between soil water and hot events/droughts. These results further implied that both droughts and hot events could promote soil water scarcity. This was consistent with the observations that droughts can cut off a region's water supply by reducing precipitation and that high temperature can reinforce evaporation. In addition, droughts usually presented a higher risk than hot events, although the risk posed by droughts and hot events varied from place to place. For example the second highest risk caused by hot events was observed in AB (0.39), but droughts had the minimal impact on soil water (0.38) there. We also noted "high–high" patterns across the BB (i.e. the conditional probabilities were 0.42 for hot events and 0.57 for droughts), which indicated that this region was vulnerable to both droughts and hot events. This phenomenon may be attributed to differences in regional climate, the type of underlying surface and soil properties, which were the main factors that influence drought propagation (Wu et al., 2018; Peña-Gallardo et al., 2019). Nonetheless, the risk caused by CEDHs ranged from 0.51 to 0.74 among different basins, which was significantly higher than any risk caused by univariate extreme events. The spatial patterns of risk associated with CEDHs was shown in Fig. 11, and indicated that there was a significantly increased risk associated with the strengthening of CEDHs. For example, grids with risk factors>0.6 comprised 65.7%, 88.3%, and 93.0% of all studied grids for moderate, severe, and extreme level events, respectively. Moreover, the, BB, GB, HB, QB and part of the INNB showed high risk levels for soil water scarcity under CEDH. As shown in Fig. 12, in terms of entire TP, the average risk caused by moderate, severe, and extreme hot events, were 0.35, 0.40, and 0.43, respectively. The risk factors were respectively

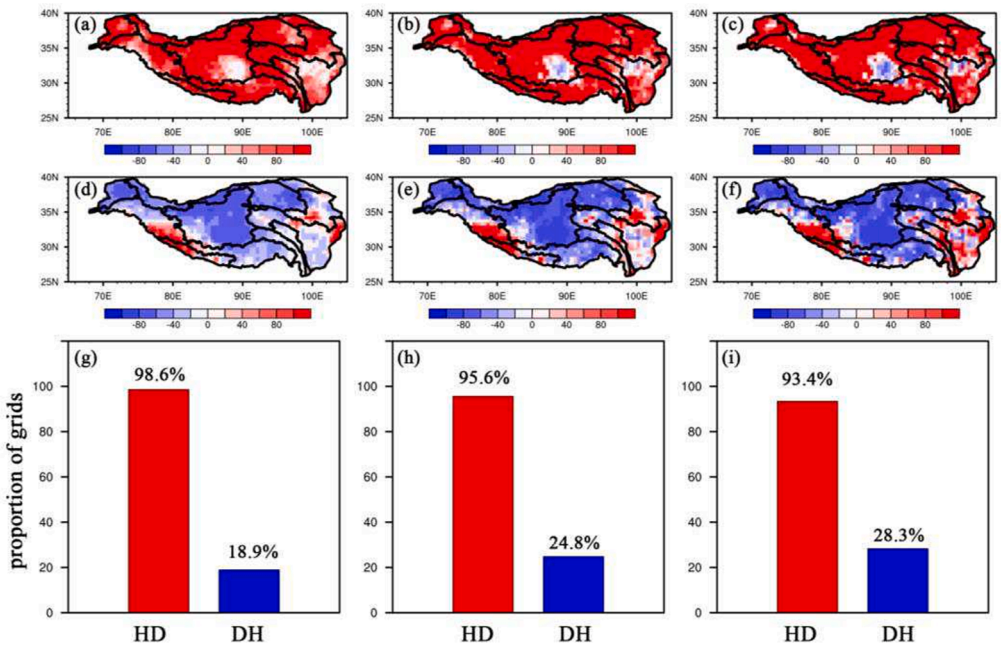

Fig. 8. The increase (%) in the conditional probability of hot under dry conditions (P (STI > thresholdSTI | SPI < thresholdSPI)) for moderate, severe and extreme level (a-c) and the increase (%) in the conditional probability of dry under hot conditions (P (SPI < thresholdSPI | STI > thresholdSTI)) (d-f) as well as the proportions of grids with increasing conditional probability. The average over all datasets was shown. Abbreviations were as follows: HD indicating (P (STI > thresholdSTI | SPI < thresholdSPI)); DH indicating (P (SPI < thresholdSPI | STI > thresholdSTI)).

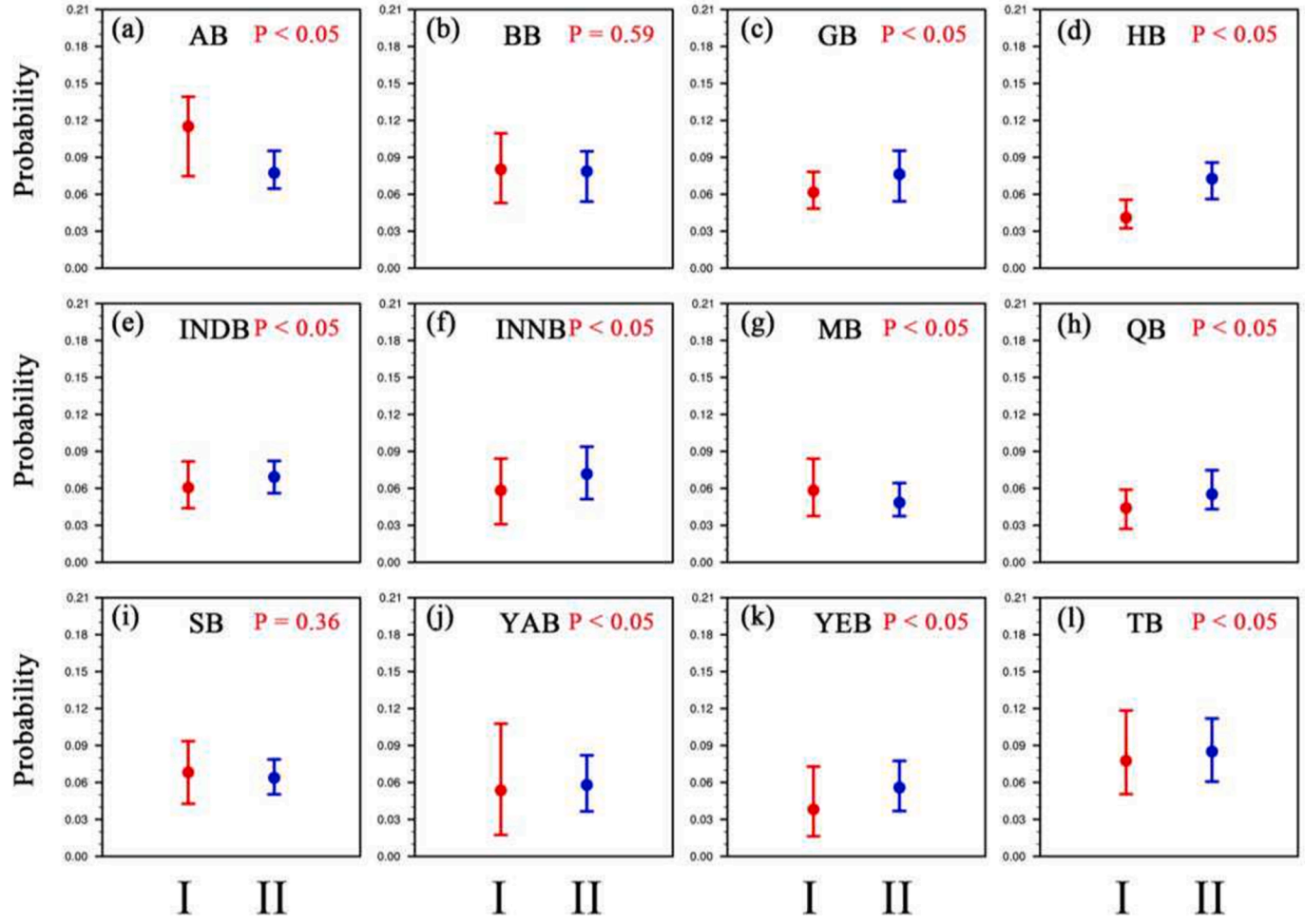

Fig. 9. Equivalent to Fig. 7, but for the "detrended" scenario.

Table 3
Equivalent to Table 2, but for the "detrended" scenario.

Basins	STI	SPI	Dependence	offset
AB	−23.5%	4.8%	−21.3%	15.4%
BB	5.3%	−7.6%	−2.5%	3.1%
GB	2.4%	20.6%	−6.3%	−27.1%
HB	−0.1%	18.3%	26.0%	−40.7%
INDB	10.1%	7.3%	13.6%	−49.8%
INNB	7.6%	23.4%	−14.1%	−43.0%
MB	−26.5%	21.2%	−11.3%	23.8%
QB	1.0%	17.7%	−4.8%	−47.1%
SB	−7.5%	10.0%	−2.7%	18.1%
YAB	−19.8%	12.9%	13.8%	−9.9%
YEB	−9.0%	−3.6%	45.8%	−22.1%
TB	−6.7%	15.4%	−2.5%	−13.3%

Table 4
Average SPI and STI values for climate extremes with long return periods (>20 years). The red numbers indicated droughts or hot events reached the moderate severity level.

	1951–1982		1983–2014	
Basins	SPI	STI	SPI	STI
AB	−1.70	0.81	−0.89	1.65
BB	−1.60	0.62	−1.09	1.53
GB	−1.32	0.72	−1.16	1.42
HB	−1.41	0.46	−0.66	1.49
INDB	−1.29	0.75	−0.98	1.41
INNB	−1.57	0.47	−0.74	1.36
MB	−1.01	0.74	−1.12	1.04
QB	−1.44	0.19	−0.50	1.37
SB	−1.23	0.90	−1.08	1.30
YAB	−1.08	0.73	−1.02	1.15
YEB	−0.96	0.64	−0.75	1.27
TB	−1.56	0.48	−0.79	1.53

0.52, 0.62, and 0.67 when moderate, severe, and extreme droughts happened. Moreover the values were 0.64, 0.75 and 0.80 for CEDHs with different severity. Furthermore, the average risk factor under moderate, severe, and extreme CEDHs increased by 81.8%, 87.4%, and 85.5%, respectively, compared with that under the hot events, and increased by 24.4%, 21.4%, and 19.0%, respectively, compared with that under droughts. The results for each grid on TP were shown in Fig. S10, the increased risk caused by CEDHs could be seen on the whole TP. In general, these results indicated that CEDHs further exacerbated soil water scarcity in comparison with droughts or hot events alone, which was consistent with the proposition that CEDHs might be more impactful than uni-variate events in isolation (Matiu et al., 2017; Feng et al., 2021a, Feng et al., 2021b).

6. Discussion

6.1. Implications

In this study, we surveyed variations of CEDHs and assessed the risk of soil water scarcity under CEDHs from a joint probability perspective; The fact that dependence between precipitation and temperature can significantly effect the probability of CEDHs was observed on TP. Positive dependence meant that there are some land–atmosphere interactions limiting the occurrence of CEDHs in some regions such as QB and YEB. The most regions on TP were still dominated by negative dependence, however, this negative dependence on TP are not as strong as other low elevation areas such as eastern China (Kong et al., 2020). This may be due to physical mechanisms that promoted or suppressed the foemation of CEDHs both existed on TP for complex climate and unique geographical characteristics on TP, finally leading to negative dependence to be offset a lot. Additionally, the combination of warming and wetting trends were also found to lessen the negative dependence.

CEDHs on TP experienced a significant rise in past 64 years for the surge in the hot events caused by a strong temperature increase signal. It was worth noting that long - term trends not only influence the

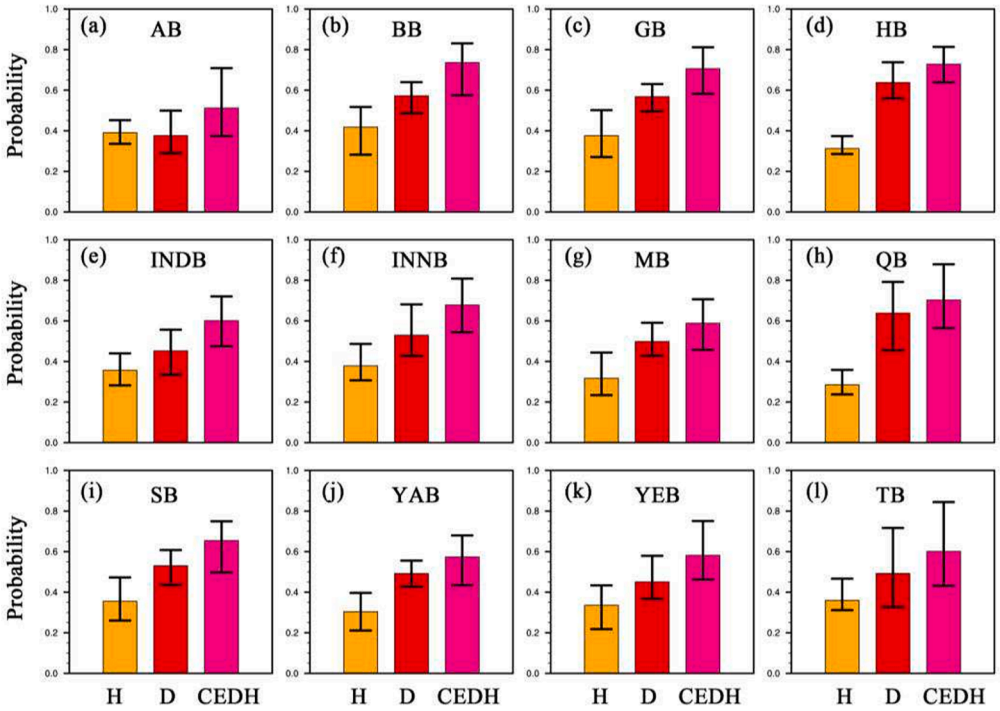

Fig. 10. The risk of water scarcity under moderate droughts (P (SSMI < -0.8 | SPI < − 0.8)), hot events (P (SSMI < -0.8 | STI > 0.8)), and CEDHs (P(SSMI < -0.8 | SPI < − 0.8 and STI > 0.8)). The average over all datasets was shown. Abbreviations were as follows: H indicating hot events, D indicating droughts, and CEDH indicating CEDHs.

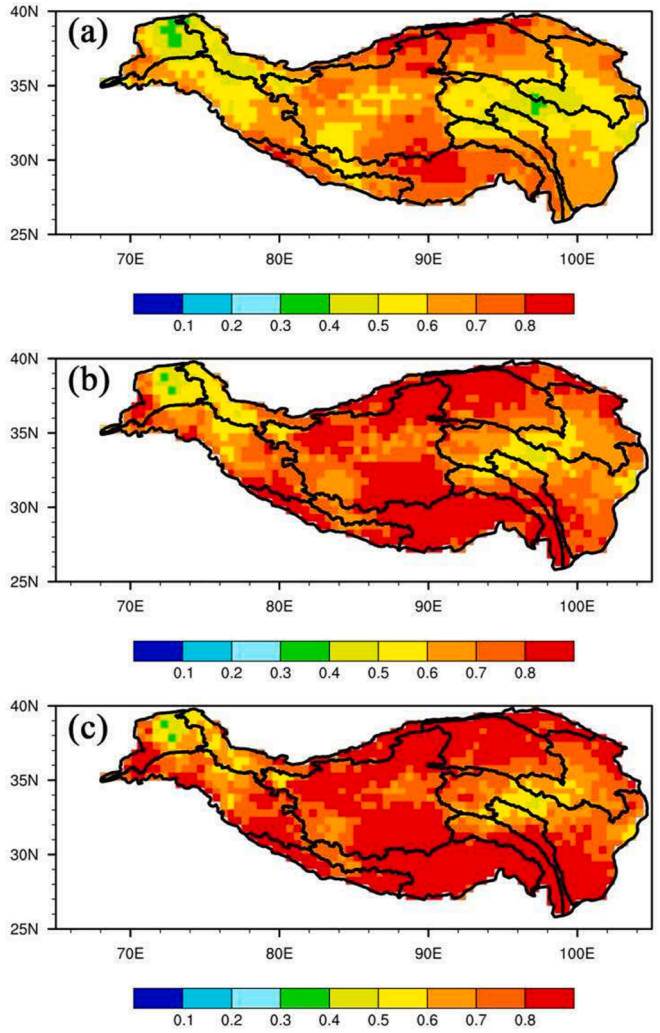

Fig. 11. The risk of water scarcity under CEDHs for moderate (a), severe (b), and extreme (c) severity levels. The average over all datasets was shown.

distribution of SPI and STI but also the dependence between them as mentioned above. Thus the contributions made from dependence might not fully reflect the role of land–atmosphere interactions. Moreover, the long-term trends were major climate change signals that might mask the role of other changes in temperature and precipitation (.e.g some multidecadal variations caused by large-scale circulation anomalies). So, the contributions based on detrended data were further investigated. The results exhibited contributions made from three factors were similar in size, emphasizing the the important role of both land–atmosphere interactions and large-scale circulation anomalies played in variations of CEDHs.

The summer is the vegetation growth season and high gross primary production (GPP) usually matches with this season (Chen et al., 2019b), however, soil water scarcity generally lead to the drop of GPP and destroy the ecosystem (Green et al., 2019; Wang et al., 2021a). Thus, soil water in summer is an important indicator to determine the growth status of vegetation and it is critical to assess the risk of soil water scarcity under CEDHs. It has been known that the real physical connection between the two variables might be contaminated by long - term trends, thus detrened process was conducted before risk assessment (Liu et al., 2018). Our results presented CEDHs generally lead to more risk of soil water scarcity than droughts or hot events do, meaning that CEDHs could attack the regional ecosystem in a more destructive way. This was consistent with previous conclusions that the high sensitivity ecosystems in arid and semi-arid regions showed to droughts and high temperatures (Peng et al 2013; Zhang et al., 2015; Papagiannopoulou et al., 2017; Hao et al., 2021). Moreover, the increasing trends of vegetation on TP has been detected (Yao et al., 2019), suggesting that vegetation would suffer greater losses under CEDHs. As a result, the CEDHs are still hot spot for this regions.

6.2. *Limitations and uncertainties*

There are also some limitations and uncertainties that exist in this study. For example, the climate datasets merging the site observations were employed in this study according to the recommendations of previous work (Yang et al., 2018; You et al., 2019; Shi et al., 2019; Wang et al., 2021c; Wei et al., 2021), but there is a fact that the observation sites on TP are unevenly distributed for its higher altitudes and harsher natural conditions, which inevitably produced bias and uncertainty. Since the soil moisture were obtained from simulations of land surface models, the uncertainty is also introduced by parameters of models. Although many soil moisture observation networks were established (Ma et al., 2020), there was still a lack of high quality observation data of soil moisture in both space and time. Consequently, high-precision and long-term datasets that cover the TP are urgently needed for further climate and hydrology research.

Risk assessments conducted in this study also had some limitations. For example, we only assessed the risk caused by climate extremes to ecosystems from the concept of soil water stress, whereas high temperatures,in fact, influence on vegetation in different way. For instance, high temperature can directly impact photosynthesis and respiration by influencing enzyme activities ((Zhu et al., 2021b)). As such, the risks presented in our study had some uncertainty. In addition, we only considered the risk of CEDH-related soil water shortage that occurred at the same time with CEDHs, even if many researches had shown that soil water shortage may last longer and harder to recover (Ding et al., 2021; Yang et al., 2022). Therefore, the risk caused by CEDHs might be underestimated. Based on the above limitations, future research will be conducted using multi-source data as well as climate models.

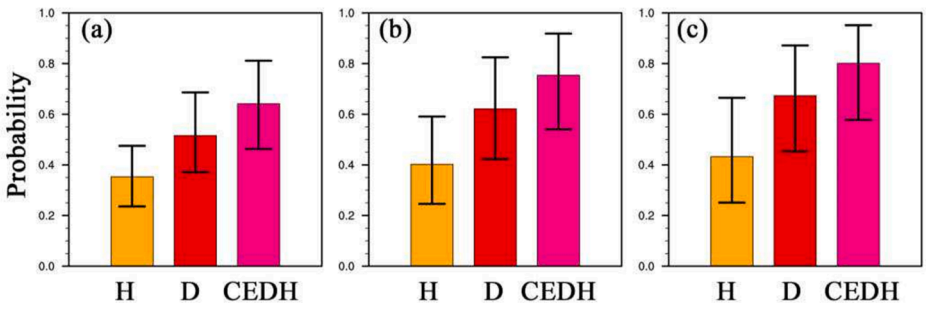

Fig. 12. The risk of water scarcity under droughts, hot events and CEDHs with different severity for whole TP. (a) Moderate level; (b) Severe level; (c) Extreme level. Abbreviations were as follows: H indicating hot events, D indicating droughts, and CEDH indicating CEDHs. The average over all datasets was shown.

7. Conclusion

Based on grid data obtained from the GPCC, CRU, PMFD and GLDAS, this study investigated spatio-temporal variations in the CEDHs and assessed the risk of soil water scarcity under CEDHs from the perspective of joint probability analysis. This was achieved by using a copula probability model to calculate the joint probability of multiple variables (SPI and STI) and the conditional probability of soil water scarcity under different scenarios (i.e. droughts, hot events, and CEDHs). The main findings are summarized below.

(1) The probability of hot events in the early period (1951–1982) was much lower than in the later period (1983–2014) across the entire TP. By contrast, the probability of droughts in the later period decreased in most basins, which were related to warming and wetting trends across the TP.
(2) The probability of CEDHs on TP increased significantly in the past 64 years due to a significant increase in hot events;
(3) In the recent 64 years, extreme events with long return periods (>20 year) generally transformed from droughts to CEDHs or hot events for the impact of temperature on the probability of extreme events became more obvious.
(4) The risk of soil water scarcity under CEDHs with different severity increased by 81.8%, 87.4%, and 85.5%, compared with that under the hot events, and increased by 24.4%, 21.4%, and 19.0%, compared with that under droughts. This indicated CEDHs could pose a greater threat to the ecosystem on TP.

CRediT authorship contribution statement

Di Wu: Methodology, Software, Writing – review & editing. **Zeyong Hu:** Conceptualization, Funding acquisition.

Declaration of Competing Interest

The authors declare that they have no known competing financial interests or personal relationships that could have appeared to influence the work reported in this paper.

Data availability

Data will be made available on request.

Acknowledgement:

This research supported by the Second Tibetan Plateau Scientific Expedition and Research (STEP) program (grant no. 2019QZKK0103), the Strategic Priority Research Program of the Chinese Academy of Sciences (grant no. XDA20060101), the National Natural Science Foundation of China (grant no. 91837208), the Systematic Major Project of the China Railway (grant no.P2021G047).

Appendix A. Supplementary data

Supplementary data to this article can be found online at https://doi.org/10.1016/j.ecolind.2023.110413.

References

Aas, K., Czado, C., Frigessi, A., Bakken, H., 2009. Pair-copula constructions of multiple dependence. Insurance Math. Econom. 44 (2), 182–198.
Asong, Z.E., Wheater, H.S., Bonsal, B., et al., 2018. Historical drought patterns over couldada and their teleconnections with large-scale climate signals. Hydrol. Earth Syst. Sci. 22 (6), 3105–3124.
Bai, W., Chen, X., Tang, Y., He, Y., Zheng, Y., 2019. Temporal and spatial changes of soil moisture and its response to temperature and precipitation over the Tibetan Plateau. Hydrol. Sci. J. 64 (11), 1370–1384.
Bastos, A., Orth, R., Reichstein, M., Ciais, P., Viovy, N., Zaehle, S., Anthoni, P., Arneth, A., Gentine, P., Joetzjer, E., Lienert, S., Loughran, T., McGuire, P.C., O, S., Pongratz, J., Sitch, S., 2021. Vulnerability of European ecosystems to two compound dry and hot summers in 2018 and 2019. Earth Syst. Dyn. 12 (4), 1015–1035.
Beniston, M., 2009. Trends in joint quantiles of temperature and precipitation in Europe since 1901 and projected for 2100. Geophys. Res. Lett. 36 (7), n/a–n/a.
Bevacqua, E., Vousdoukas, M.I., Zappa, G., Hodges, K., Shepherd, T.G., Maraun, D., Mentaschi, L., Feyen, L., 2020. More meteorological events that drive compound coastal flooding are projected under climate change. Communications earth & environment 1 (1).
Bogner, K., Pappenberger, F., Cloke, H.L., 2012. The normal quantile transformation and its application in a flood forecasting system. Hydrol. Earth Syst. Sci. 16 (4), 1085–1094.
Chen, L., Chen, X., Cheng, L., Zhou, P., Liu, Z., 2019a. Compound hot droughts over China: Identification, risk patterns and variations. Atmos. Res. 227, 210–219.
Chen, D.L., Xu, B., Yao, T.D., et al., 2015. Assessment of past, present and future environmental changes on the Tibetan Plateau. Chin. Sci. Bull. 60 (32).
Chen, W., Zhu, D., Huang, C., Ciais, P., Yao, Y., Friedlingstein, P., Sitch, S., Haverd, V., Jain, A.K., Kato, E., Kautz, M., Lienert, S., Lombardozzi, D., Poulter, B., Tian, H., Vuichard, N., Walker, A.P., Zeng, N., 2019b. Negative extreme events in gross primary productivity and their drivers in China during the past three decades. Agric. For. Meteorol. 275, 47–58.
Ding, Y., Gong, X., Xing, Z., Cai, H., Zhou, Z., Zhang, D., Sun, P., Shi, H., 2021. Attribution of meteorological, hydrological and agricultural drought propagation in different climatic regions of China. Agric Water Manag 255, 106996.
Fang, K., Makkonen, R., Guo, Z., Zhao, Y., Seppä, H., 2015. An increase in the biogenic aerosol concentration as a contributing factor to the recent wetting trend in Tibetan Plateau. Sci. Rep. 5 (1).
Feng, S., Hao, Z., Zhang, X., Hao, F., 2019. Probabilistic evaluation of the impact of compound dry-hot events on global maize yields. Sci. Total Environ. 689, 1228–1234.
Feng, S., Hao, Z., Wu, X., Zhang, X., Hao, F., 2021a. A multi-index evaluation of changes in compound dry and hot events of global maize areas. J. Hydrol. 602, 126728.
Feng, Y., Liu, W., Sun, F., et al., 2021b. Changes of compound hot and dry extremes on different land surface conditions in China during 1957–2018. Int. J. Climatol. 41, E1085–E1099.
Feng, S, Wu, X, Hao, Z, et al., 2020. A database for characteristics and variations of global compound dry and hot events[J]. Weather and Climate Extremes 30, 100299.
Fischer, E.M., Schär, C., 2010. Consistent geographical patterns of changes in high-impact European heatwaves. Nat. Geosci. 3 (6), 398–403.
Fu, G., Zhang, X., Zhang, Y., Shi, P., Li, Y., Zhou, Y., Yang, P., Shen, Z., 2013. Experimental warming does not enhance gross primary production and above-ground biomass in the alpine meadow of Tibet. J. Appl. Remote Sens. 7 (1), 073505.
Ganguli, P., 2022. Amplified risk of compound heat stress-dry spells in Urban India. Clim. Dyn. 1–18.
Green, J.K., Seneviratne, S.I., Berg, A.M., Findell, K.L., Hagemann, S., Lawrence, D.M., Gentine, P., 2019. Large influence of soil moisture on long-term terrestrial carbon uptake. Nature 565 (7740), 476–479.
Gringorten, I.I., 1963. A simplified method of estimating extreme values from data samples. J. Appl. Meteorol. Climatol. 2 (1), 82–89.
Hao, Z., AghaKouchak, A., Phillips, T.J., 2013. Changes in concurrent monthly precipitation and temperature extremes. Environ. Res. Lett. 8 (3), 034014.
Hao, Z., Hao, F., Singh, V.P., Zhang, X., 2018. Changes in the severity of compound drought and hot extremes over global land areas. Environ. Res. Lett. 13 (12), 124022.
Hao, Z., Hao, F., Xia, Y., Singh, V.P., Zhang, X., 2019. A monitoring and prediction system for compound dry and hot events. Environ. Res. Lett. 14 (11), 114034.
Hao, Y., Hao, Z., Fu, Y., Feng, S., Zhang, X., Wu, X., Hao, F., 2021. Probabilistic assessments of the impacts of compound dry and hot events on global vegetation during growing seasons. Environ. Res. Lett. 16 (7), 074055.
Hao, Z., Li, W., Singh, V.P., Xia, Y., Zhang, X., Hao, F., 2020a. Impact of dependence changes on the likelihood of hot extremes under drought conditions in the United States. J. Hydrol. 581, 124410.
Hao, Z., Zhang, X., Singh, V.P., Hao, F., 2020b. Joint modeling of precipitation and temperature under influences of El Niño Southern Oscillation for compound event evaluation and prediction. Atmos. Res. 245, 105090.
Hua, T., Wang, X., 2018. Temporal and spatial variations in the climate controls of vegetation dynamics on the Tibetan Plateau during 1982–2011. Adv. Atmos. Sci. 35 (11), 1337–1346.
Huang, W., Prokhorov, A., 2014. A goodness-of-fit test for copulas. Econ. Rev. 33 (7), 751–771.
Kollanus, V., Tiittanen, P., Lanki, T., 2021. Mortality risk related to heatwaves in Finland-Factors affecting vulnerability. Environ. Res. 201, 111503.
Kong, Q., Guerreiro, S.B., Blenkinsop, S., Li, X.-F., Fowler, H.J., 2020. Increases in summertime concurrent drought and heatwave in Eastern China. Weather Clim. Extremes 28, 100242.
Lai, C., Li, J., Wang, Z., Wu, X., Zeng, Z., Chen, X., Lian, Y., Yu, H., Wang, P., Bai, X., 2018. Drought-induced reduction in net primary productivity across mainland China from 1982 to 2015. Remote Sens. (Basel) 10 (9), 1433.
Li, X., Li, Y., Chen, A., Gao, M., Slette, I.J., Piao, S., 2019b. The impact of the 2009/2010 drought on vegetation growth and terrestrial carbon balance in Southwest China. Agric. For. Meteorol. 269-270, 239–248.
Li, H.W., Li, Y.P., Huang, G.H., Sun, J., 2021. Quantifying effects of compound dry-hot extremes on vegetation in Xinjiang (China) using a vine-copula conditional probability model. Agric. For. Meteorol. 311, 108658.

Li, H., Shen, W., Zou, C., Jiang, J., Fu, L., She, G., 2013. Spatio-temporal variability of soil moisture and its effect on vegetation in a desertified aeolian riparian ecotone on the Tibetan Plateau, China. J. Hydrol. 479, 215–225.
Li, H., Liu, L., Shan, B., Xu, Z., Niu, Q., Cheng, L., Liu, X., Xu, Z., 2019a. Spatiotemporal variation of drought and associated multi-scale response to climate change over the Yarlung Zangbo River Basin of Qinghai-Tibet Plateau, China. Remote Sens. (Basel) 11 (13), 1596.
Li, P., Zhu, D., Wang, Y., Liu, D., 2020. Elevation dependence of drought legacy effects on vegetation greenness over the Tibetan Plateau. Agric. For. Meteorol. 295, 108190.
Lin, Z, Yao, X, Guo, W, et al., 2021. Vertical structure of Tibetan Plateau Vortex in boreal summer[J]. Theoretical and Applied Climatology 145 (1–2), 427–440.
Liu, Y., Liu, Y., Wang, W., et al., 2022. Historical droughts manifest an abrupt shift to a wetter Tibetan Plateau. Hydrol. Earth Syst. Sci. Discuss. 1–29.
Liu, L., Peng, S., AghaKouchak, A., Huang, Y., Li, Y., Qin, D., Xie, A., Li, S., 2018. Broad consistency between satellite and vegetation model estimates of net primary productivity across global and regional scales. J. Geophys. Res. Biogeo. 123 (12), 3603–3616.
Liu, W., Sun, F., Feng, Y., Li, C., Chen, J., Sang, Y.-F., Zhang, Q., 2021. Increasing population exposure to global warm-season concurrent dry and hot extremes under different warming levels. Environ. Res. Lett. 16 (9), 094002.
Ma, Y., Hu, Z., Xie, Z., Ma, W., Wang, B., Chen, X., Li, M., Zhong, L., Sun, F., Gu, L., Han, C., Zhang, L., Liu, X., Ding, Z., Sun, G., Wang, S., Wang, Y., Wang, Z., 2020. A long-term (2005–2016) dataset of hourly integrated land–atmosphere interaction observations on the Tibetan Plateau. Earth Syst. Sci. Data 12 (4), 2937–2957.
Manning, C., Widmann, M., Bevacqua, E., Van Loon, A.F., Maraun, D., Vrac, M., 2019. Increased probability of compound long-duration dry and hot events in Europe during summer (1950–2013). Environ. Res. Lett. 14 (9), 094006.
Matiu, M, Ankerst, D P, Menzel, A, 2017. Interactions between temperature and drought in global and regional crop yield variability during 1961-2014[J]. PloS one 12 (5), e0178339.
Mazdiyasni, O, AghaKouchak, A, 2015. Substantial increase in concurrent droughts and heatwaves in the United States[J]. Proceedings of the National Academy of Sciences 112 (37), 11484–11489.
Nelsen, R.B., 2007. An introduction to copulas[M]. Springer Science & Business. Media.
Papagiannopoulou, C., Miralles, D.G., Dorigo, W.A., Verhoest, N.E.C., Depoorter, M., Waegeman, W., 2017. Vegetation anomalies caused by antecedent precipitation in most of the world. Environ. Res. Lett. 12 (7), 074016.
Peña-Gallardo, M, Vicente-Serrano, S M, Hannaford, J, et al., 2019. Complex influences of meteorological drought time-scales on hydrological droughts in natural basins of the contiguous Unites States[J]. Journal of Hydrology 568, 611–625.
Peng, S., Piao, S., Shen, Z., Ciais, P., Sun, Z., Chen, S., Bacour, C., Peylin, P., Chen, A., 2013. Precipitation amount, seasonality and frequency regulate carbon cycling of a semi-arid grassland ecosystem in Inner Mongolia, China: A modeling analysis. Agric. For. Meteorol. 178-179, 46–55.
Perkins, S.E., Alexander, L.V., Nairn, J.R., 2012. Increasing frequency, intensity and duration of observed global heatwaves and warm spells. Geophys. Res. Lett. 39 (20).
Qin, Y., Yang, D., Lei, H., Xu, K., Xu, X., 2015. Comparative analysis of drought based on precipitation and soil moisture indices in Haihe basin of North China during the period of 1960–2010. J. Hydrol. 526, 55–67.
YOU, Qinglong, KANG, Shichang, LI, Jiandong, CHEN, Deliang, ZHAI, Panmao, JI, Zhenming, 2021. Several research frontiers of climate change over the Tibetan Plateau[J]. Journal of Glaciology and Geocryology 43 (3), 885–901.
Qiu, Y., Fu, B.J., Wang, J., Zhang, X.L., Meng, Q.H., 2007. Spatiotemporal variation of soil moisture and its relation to environmental factors. Chin. J. Ecol. 1, 100–107 (in Chinese).
Robine, J.-M., Cheung, S.L.K., Le Roy, S., Van Oyen, H., Griffiths, C., Michel, J.-P., Herrmann, F.R., 2008. Death toll exceeded 70,000 in Europe during the summer of 2003. C. R. Biol. 331 (2), 171–178.
Sheffield, J., Goteti, G., Wood, E.F., 2006. Development of a 50-year high-resolution global dataset of meteorological forcings for land surface modeling. J. Clim. 19 (13), 3088–3111.
Shi, C., Shen, M., Wu, X., Cheng, X., Li, X., Fan, T., Li, Z., Zhang, Y., Fan, Z., Shi, F., Wu, G., 2019. Growth response of alpine treeline forests to a warmer and drier climate on the southeastern Tibetan Plateau. Agric. For. Meteorol. 264, 73–79.
Sun, H., Chen, Y., Xiong, J., Ye, C., Yong, Z., Wang, Y.i., He, D., Xu, S., 2022. Relationships between climate change, phenology, edaphic factors, and net primary productivity across the Tibetan Plateau. Int. J. Appl. Earth Obs. Geoinf. 107, 102708.
Wan, W., Long, D.i., Hong, Y., Ma, Y., Yuan, Y., Xiao, P., Duan, H., Han, Z., Gu, X., 2016. A lake data set for the Tibetan Plateau from the 1960s, 2005, and 2014. Sci. Data 3 (1).
Wang, S.-Y., Kim, H., Coumou, D., Yoon, J.-H., Zhao, L., Gillies, R.R., 2019b. Consecutive extreme flooding and heat wave in Japan: Are they becoming a norm? Atmos. Sci. Lett. 20 (10), e933.
Wang, S., Liu, F., Zhou, Q., et al., 2021c. Drought evolution characteristics of the Qinghai-Tibet Plateau over the last 100 years based on SPEI. Nat. Hazards Earth Syst. Sci. Discuss. 1–20.
Wang, R., Lü, G., Ning, L., Yuan, L., Li, L., 2021b. Likelihood of compound dry and hot extremes increased with stronger dependence during warm seasons. Atmos. Res. 260, 105692.
Wang, M., Wang, S., Zhao, J., Ju, W., Hao, Z., 2021a. Global positive gross primary productivity extremes and climate contributions during 1982–2016. Sci. Total Environ. 774, 145703.
Wang, X., Yi, S., Wu, Q., Yang, K., Ding, Y., 2016. The role of permafrost and soil water in distribution of alpine grassland and its NDVI dynamics on the Qinghai-Tibetan Plateau. Global Planet. Change 147, 40–53.
Wei, Y., Lu, H., Wang, J., Wang, X., Sun, J., 2022. Dual influence of climate change and anthropogenic activities on the spatiotemporal vegetation dynamics over the Qinghai-Tibetan Plateau from 1981 to 2015. Earth's. Future 10 (5).
White, H., 1982. Maximum likelihood estimation of misspecified models. Econometrica 50 (1), 1.
Wu, X., Jiang, D., 2022. Probabilistic impacts of compound dry and hot events on global gross primary production. Environ. Res. Lett. 17 (3), 034049.
Wu J, Miao C, Zheng H, et al. Meteorological and hydrological drought on the Loess Plateau, China: Evolutionary characteristics, impact, and propagation[J]. Journal of Geophysical Research: Atmospheres, 2018, 123(20): 11,569-11,584.
Xiao, M., Zhang, Q., Singh, V.P., Liu, L., 2016. Transitional properties of droughts and related impacts of climate indices in the Pearl River basin, China. J. Hydrol. 534, 397–406.
Yang, F., Duan, X., Guo, Q., Lu, S., Hsu, K., 2022. The spatiotemporal variations and propagation of droughts in Plateau Mountains of China. Sci. Total Environ. 805, 150257.
Yang, K., Lu, H., Yue, S., Zhang, G., Lei, Y., La, Z., Wang, W., 2018. Quantifying recent precipitation change and predicting lake expansion in the Inner Tibetan Plateau. Clim. Change 147 (1-2), 149–163.
Yao, T., Xue, Y., Chen, D., Chen, F., Thompson, L., Cui, P., Koike, T., Lau, W.-M., Lettenmaier, D., Mosbrugger, V., Zhang, R., Xu, B., Dozier, J., Gillespie, T., Gu, Y.u., Kang, S., Piao, S., Sugimoto, S., Ueno, K., Wang, L., Wang, W., Zhang, F., Sheng, Y., Guo, W., Ailikun, Yang, X., Ma, Y., Shen, S.S.P., Su, Z., Chen, F., Liang, S., Liu, Y., Singh, V.P., Yang, K., Yang, D., Zhao, X., Qian, Y., Zhang, Y.u., Li, Q., 2019. Recent third pole's rapid warming accompanies cryospheric melt and water cycle intensification and interactions between monsoon and environment: Multidisciplinary approach with observations, modeling, and analysis. Bull. Americould Meteorol. Soc. 100 (3), 423–444.
Yin, H., Sun, Y., Donat, M.G., 2019. Changes in temperature extremes on the Tibetan Plateau and their attribution. Environ. Res. Lett. 14 (12), 124015.
You, G., Arain, M.A., Wang, S., McKenzie, S., Zou, C., Wang, Z., Li, H., Liu, B.o., Zhang, X., Gu, Y., Gao, J., 2019. The spatial-temporal distributions of controlling factors on vegetation growth in Tibet Autonomous Region, Southwestern China. Environ. Res. Commun. 1 (9), 091003.
You, Q., Kang, S., Aguilar, E., Yan, Y., 2008. Changes in daily climate extremes in the eastern and central Tibetan Plateau during 1961–2005. J. Geophys. Res. Atmos. 113 (D7).
Zhang, G., 2019. Dataset of river basins map over the TP(2016). National Tibetan Plateau Data Center.
Zhang, Y.u., Hao, Z., Feng, S., Zhang, X., Hao, F., 2022. Changes and driving factors of compound agricultural droughts and hot events in eastern China. Agric Water Manag 263, 107485.
Zhang, Y., Voigt, M., Liu, H., 2015. Contrasting responses of terrestrial ecosystem production to hot temperature extreme regimes between grassland and forest. Biogeosciences 12 (2), 549–556.
Zhang, G., Yao, T., Xie, H., Kang, S., Lei, Y., 2013. Increased mass over the Tibetan Plateau: From lakes or glaciers? Geophys. Res. Lett. 40 (10), 2125–2130.
Zhao, W.Z., 2002. Impact of plantation on spatial variability of soil moisture in Horqin sandy land. Acta Pedol. Sin. 1, 113–1191 in Chinese.
Zhu, Y.e., Liu, ·Yi, Wang, W., Singh, V.P., Ren, L., 2021a. A global perspective on the probability of propagation of drought: From meteorological to soil moisture. J. Hydrol. 603, 126907.
Zhu, X., Zhang, S., Liu, T., Liu, Y., 2021b. Impacts of heat and drought on gross primary productivity in China. Remote Sens. (Basel) 13 (3), 378.
Zscheischler, J., Seneviratne, S.I., 2017. Dependence of drivers affects risks associated with compound events. Sci. Adv. 3 (6), e1700263.

Further reading

Barriopedro, D., Fischer, E.M., Luterbacher, J., Trigo, R.M., García-Herrera, R., 2011. The hot summer of 2010: redrawing the temperature record map of Europe. Science 332 (6026), 220–224.
van der Schrier, G., Barichivich, J., Briffa, K.R., Jones, P.D., 2013. A scPDSI-based global data set of dry and wet spells for 1901–2009. J. Geophys. Res. Atmos. 118 (10), 4025–4048.
Wang, Q., Yang, Y., Liu, Y., Tong, L., Zhang, Q.-P., Li, J., 2019a. Assessing the impacts of drought on grassland net primary production at the global scale. Sci. Rep. 9 (1).
Yao, T., Bolch, T., Chen, D., et al., 2022. The imbalance of the Asian water tower. Nat. Rev. Earth Environ. 1–15.